Open Research Online

Two-photon state selection and angular momentum polarization probed by velocity map imaging: Application to H atom photofragment angular distributions from the photodissociation of two-photon state selected HCl and HBr

Journal Item

oro.open.ac.uk

Two-photon state selection and angular momentum polarization probed by velocity map imaging: Application to H atom photofragment angular distributions from the photodissociation of two-photon state selected HCl and HBr

Sergei Manzhos, Constantin Romanescu, and Hans-Peter Loock
Department of Chemistry, Queen's University, Kingston, Ontario K7L 3N6, Canada

Jonathan G. Underwood[a)]
Department of Physics and Astronomy, The Open University, Walton Hall, Milton Keynes, MK7 6AA, United Kingdom

A formalism for calculating the angular momentum polarization of an atom or a molecule following two-photon excitation of a *J*-selected state is presented. This formalism is used to interpret the H atom photofragment angular distributions from single-photon dissociation of two-photon rovibronically state selected HCl and HBr prepared via a *Q*-branch transition. By comparison of the angular distributions measured using the velocity map imaging technique with the theoretical model it is shown that single-photon dissociation of two-photon prepared states can be used for pathway identification, allowing for the identification of the virtual state symmetry in the two-photon absorption and/or the symmetry of the dissociative state. It is also shown that under conditions of excitation with circularly polarized light, or for excitation via non-*Q*-branch transitions with linearly polarized light the angular momentum polarization is independent of the dynamics of the two-photon transition and analytically computable. © *2004 American Institute of Physics.*
[DOI: 10.1063/1.1809571]

I. INTRODUCTION

The measurement of photofragment angular distributions following single-photon photodissociation of an isotropically distributed ensemble of ground state molecules can provide substantial detail regarding the electronic symmetries of the dissociative state(s), the orientation of the transition dipole moment in the molecular frame, the subsequent dissociation time scales, and the electronic and nuclear dynamics.[1–4] Sensitive experimental methods for probing photofragment angular distributions have been developed including the measurement of Doppler and time-of-flight profiles,[1,5–8] and more recently, velocity map imaging.[9,10] These techniques have also been extended to allow for the probing of the vector correlation between the velocity and the angular momentum polarization of the photofragments, and the extraction of more detailed information regarding the dissociation dynamics and the interference effects resulting from coherent excitation to multiple dissociative electronic states.[5,11]

While these increasingly differential measurements of photodissociation product state distributions and vector correlations yield great insight into the photofragmentation process, it is also advantageous to remove the averaging over the initially populated states of the parent molecules. This can be achieved through state selection of the parent molecules via optical excitation prior to photodissociation. In principle, a rovibronic state of the parent can thereby be selected, depending on optical selection rules and the lifetime of the prepared state. Optical excitation will also lead to an ensemble of parent molecules whose angular momentum is polarized in the laboratory frame, and an associated molecular axis alignment. The effects of this prepared angular momentum polarization upon the observed vector correlations are pronounced and complicated.[12–14] Control over the prepared angular momentum polarization provides a powerful tool for the interrogation of the photodissociation dynamics, allowing for control over which electronic states are active in the photodissociation.[12,15] In essence, a state of known angular momentum polarization (and molecular axis alignment/orientation) allows for control over the molecular frame geometry in the laboratory frame and so control over the molecular frame transition dipole moment.[12,15]

To date, several techniques have been explored for the creation of well defined angular momentum polarization and molecular axis alignment including single-photon absorption,[16–18] the use of strong axis-orienting dc electric fields[19–21] and intense nonresonant axis-aligning laser fields.[22] In this paper, we discuss the use of two-photon absorption to provide state selected angular momentum polarization prior to single-photon photodissociation. In addition to providing the means for state and polarization selection, two-photon state preparation is often advantageous as a first step in accessing high lying states of the neutral and also the parent ion,[23] which would be otherwise inaccessible from the ground state due to either selection rules or available laser sources. It is necessary therefore to develop a formalism describing the angular momentum polarization produced through two-photon absorption, and this is presented in the

---

[a)]Electronic mail: j.underwood@open.ac.uk

J. Chem. Phys., Vol. 121, No. 23, 15 December 2004

Two-photon state selection   11803

following section. The problem of describing the angular momentum polarization produced through optical excitation is closely related to the similar problem of probing product angular momentum polarization[24] using methods such as laser induced fluorescence,[25–27] single-photon absorption,[28] or two-photon excitation.[29–32]

In Sec. II, we develop the formalism for describing the angular momentum polarization produced by two-photon state selection, and in Sec. III we apply this formalism to the interpretation of H atom photofragment angular distributions from single-photon photodissociation of two-photon state selected HCl ($E\,^1\Sigma^+_{0^+}$) and HBr ($H\,^1\Sigma^+_{0^+}$). We show in Sec. III that the photofragment angular distributions reflect both the photodissociation dynamics and the dynamics of the two-photon state selection. Specifically, two-photon absorption may proceed via different virtual states at the single-photon level,[33] and in the general case it is necessary to know the contributions of virtual states of different electronic symmetry to the two-photon transition amplitude in order to calculate the upper state polarization. In Sec. II, it is shown that in the specific cases of circularly polarized light, or linearly polarized light and non-Q-branch transitions, it is possible to

calculate the upper state polarization analytically without knowledge of the contributions of the different virtual states. In Sec. III, we show that the photofragment angular distributions from single-photon dissociation can be used to deduce the contributions of the different virtual state amplitudes to the two-photon cross section.

II. ANGULAR MOMENTUM POLARIZATION FROM TWO-PHOTON STATE SELECTION

In this section, we present a formalism for describing the angular momentum polarization of an atomic or rigid-rotor molecular ensemble following two-photon absorption in which a single rovibronic transition is selected. For generality, we will proceed by ignoring the details of the target angular momentum coupling scheme and represent states in the form $|JMn\rangle$, where J and M are the total angular momentum and lab frame projection quantum numbers, and n represents all other quantum numbers.

For an unpolarized ground state J_0, the density matrix describing the excited state polarization following two-photon excitation is given by

$$^{J'J}\rho_{M'M} \propto \sum_{M_0} \sum_{n_i'J_i'M_i'} \sum_{n_iJ_iM_i} \frac{\langle nJ'M'|\mathbf{d}\cdot\mathbf{e}|n_i'J_i'M_i'\rangle\langle n_i'J_i'M_i'|\mathbf{d}\cdot\mathbf{e}|n_0J_0M_0\rangle}{E_{n_i'J_i'}-E_{h\nu}+i\Gamma_{n_i'J_i'}/2} \left[\frac{\langle nJM|\mathbf{d}\cdot\mathbf{e}|n_iJ_iM_i\rangle\langle n_iJ_iM_i|\mathbf{d}\cdot\mathbf{e}|n_0J_0M_0\rangle}{E_{n_iJ_i}-E_{h\nu}+i\Gamma_{n_iJ_i}/2}\right]^*.$$

(1)

This equation allows for the possibility of upper J state coherence for the situation where the upper state is not J selected. For the situation where more than a single ground state J_0 contributes, the equation above should include an incoherent sum over these J_0 states with a suitable Boltzmann weighting factor. The two-photon absorption proceeds via an intermediate virtual state indicated by the subscript i.[30]

It is convenient to formulate an expression for the multipole moments of the excited state density matrix, where these are defined as[34]

$$^{J'J}T_{KQ} = \sum_{M'M} (-1)^{J'-M'}[K]^{1/2} \times \begin{pmatrix} J' & J & K \\ M' & -M & -Q \end{pmatrix} {}^{J'J}\rho_{M'M}.$$

(2)

Here and in what follows, we use $[A,B,\dots]$ to represent $[(2A+1)(2B+1)\cdots]$. Combining Eqs. (2) and (1) and carrying out the angular momentum algebra (see Appendix A) leads to the following expression for the multipole moments

$$^{J'J}T_{KQ} = \sum_{k_1k_2} (-1)^Q \mathcal{E}^K_{-Q}(k_1,k_2)$$

$$\times \sum_{J_iJ_i'} h(k_1,k_2,K,J_0,J,J',J_i,J_i')$$

$$\times T(J',J_i')T(J,J_i)^*.$$

(3)

Here the spherical tensor contraction $\mathcal{E}^K_{-Q}(k_1,k_2)$ contains all of the geometrical information regarding the laser polarization (see Appendix B), and the remaining geometrical factors are given by

$$h(k_1,k_2,K,J_0,J,J',J_i,J_i')$$

$$=(-1)^{J+J_0+k_1+k_2}[K,k_1,k_2]^{1/2}\begin{Bmatrix} 1 & 1 & k_1 \\ J_0 & J' & J_i' \end{Bmatrix}$$

$$\times\begin{Bmatrix} 1 & 1 & k_2 \\ J_0 & J & J_i \end{Bmatrix}\begin{Bmatrix} k_1 & k_2 & K \\ J & J' & J_0 \end{Bmatrix}.$$

(4)

The dynamical parameters are defined in terms of reduced matrix elements as

$$T(J,J_i)=\sum_{n_i}\frac{\langle nJ\|d^1\|n_iJ_i\rangle\langle n_iJ_i\|d^1\|n_0J_0\rangle}{E_{n_iJ_i}-E_{h\nu}+i\Gamma_{n_iJ_i}/2}.$$

(5)

The product $T(J',J_i')T(J,J_i)^*$ appearing in Eq. (3) will therefore introduce a coherent sum over the (currently un-

specified) quantum numbers n_i and n'_i denoting the electronic symmetry of the intermediate virtual states. The reduced matrix elements satisfy the condition

$$\langle nJ\|d^1\|n_iJ_i\rangle^* = (-1)^{J-J_i}\langle n_iJ_i\|d^1\|nJ\rangle. \tag{6}$$

The above expressions are valid for atomic or molecular targets described by angular momentum quantum numbers J and M. A number of important observations regarding these expressions may be made. From the properties of $\mathcal{E}^K_{-Q}(k_1,k_2)$, it is seen that, for linearly or circularly polarized light, only multipole moments with $Q=0$ are nonzero; elliptically polarized light will result in nonzero multipole moments also with $Q\neq0$. This is a result of the cylindrical symmetry exhibited by linearly and circularly polarized light; elliptically polarized light possesses no axis of cylindrical symmetry. Additionally, k_1 and k_2 are limited to the values $0,\dots,2$. For a state of circular polarization, k_1 and k_2 take only the value 2, whereas for linearly polarized light, k_1 and k_2 take the values 0 and 2. From the properties of the 6-j symbols in the $h(k_1,k_2,K,J_0,J,J',J_i,J'_i)$ factors, it is seen that (J_0,J',k_1) must satisfy a triangle condition, as do (J_0,J,k_2). From these triangle conditions, we find $\Delta J=0,\pm1,\pm2$ as is well known for two-photon transitions.[30] Additionally, k_1 and k_2 only take the value 0 when $J'=J_0$ and $J=J_0$, respectively. Therefore, for linearly polarized light, k_1 and k_2 take the values 0 and 2 for Q-branch transitions only, whereas for non-Q-branch transitions, k_1 and k_2 take the single value of 2.

Examining the specific case of sharp angular momentum in the upper state ($J'=J$) and $k_1=k_2=2$ only (i.e., circularly polarized light, or linearly polarized light with $J\neq J_0$), it is found that the multipole moments when normalized to $^{JJ}T_{00}=1$ take the particularly simple analytical form given below in which the (usually unknown) dynamical parameters no longer appear[32]

$$^{JJ}T_{K0} = (-1)^{J+J_0}5[K,J]^{1/2}\begin{pmatrix} 2 & 2 & K \\ 2p & -2p & 0 \end{pmatrix} \\ \times\begin{Bmatrix} J & J & K \\ 2 & 2 & J_0 \end{Bmatrix}. \tag{7}$$

Hence, for this specific but common case, one is able to calculate the excited state angular momentum polarization without requiring any knowledge of the dynamics of the two-photon transition. In the more general case, however, recourse to Eq. (3) is needed and requires a knowledge of the dynamical parameters describing the different coherent pathways contributing to the two-photon absorption. In the following section, this general case will be discussed in detail.

For a diatomic molecule, which we discuss in the following section, the reduced matrix elements are expressed for Hund's cases (a) and (c) as[30]

$$\langle n_2J_2\|d^1\|n_1J_1\rangle = \sqrt{\frac{4\pi}{3}}(-1)^{J_2-\Omega_2}[J_1,J_2]^{1/2} \\ \times\begin{pmatrix} J_1 & J_2 & 1 \\ \Omega_1 & -\Omega_2 & \Omega_2-\Omega_1 \end{pmatrix}R_{\Omega_2,\Omega_1}, \tag{8}$$

where the previously unspecified quantum number(s) n is associated with Ω, and R_{Ω,Ω_i} represents the radial dipole matrix element. For Hund's case (b), Ω is replaced with Λ.[30] Eq. (3) will therefore in general contain a coherent summation over the radial dipole matrix elements describing transitions via the different possible intermediate virtual Ω_i states at the single-photon level contained in the dynamical parameters $T(J,J_i)$,

$$T(J,J_i) = \frac{4\pi}{3}\sum_{\Omega\Omega_0}\sum_{\Omega_i}(-1)^{J-\Omega+J_i-\Omega_i}[J,J_0]^{1/2}[J_i] \\ \times\begin{pmatrix} J_i & J & 1 \\ \Omega_i & -\Omega & \Omega-\Omega_i \end{pmatrix} \\ \times\begin{pmatrix} J_0 & J_i & 1 \\ \Omega_0 & -\Omega_i & \Omega_i-\Omega_0 \end{pmatrix} \\ \times\frac{R^{(2)}_{\Omega,\Omega_i}R^{(1)}_{\Omega_i,\Omega_0}}{E_{\Omega_iJ_i}-E_{h\nu}+i\Gamma_{\Omega_iJ_i}/2}. \tag{9}$$

The superscripts (1) and (2) denote the first and second photon, respectively.

III. H ATOM PHOTOFRAGMENT ANGULAR DISTRIBUTIONS FROM PHOTODISSOCIATION OF TWO-PHOTON STATE SELECTED HCL AND HBR

In this section, we apply the theory presented above to the interpretation of the H atom photofragment angular distribution from single-photon photodissociation of two-photon rovibronically state selected HCl and HBr.

A. Experimental details

The photofragment angular distributions were measured using the velocity map imaging technique[9,10] as described previously.[13] The experiments were performed using the same linearly polarized laser pulse for the two-photon state preparation and the subsequent single-photon photodissociation of this prepared state. Two-photon rovibronic state selection was achieved using the Q-branch $J=1$ transition to the $E^1\Sigma_0$ state of HCl at 83772.0 cm^{-1}, and the $H^1\Sigma_0$ state of HBr at 79643.0 cm^{-1}. The same laser pulse also served to ionize the resulting H $2s$ and $2p$ atom photofragments which were subsequently detected using an ion imaging time of flight apparatus. Typically pulse energies of 300 μJ and 10 ns pulse duration focused to a spot size of <100 μm diameter were used. The ionization cross section for the H ($n=2$) atom photofragments was estimated to be $>4\times10^{-18}$ cm^2 for the laser wavelengths employed.[35] This large cross section for ionization under these experimental conditions ensured a large ionization rate constant of $\gtrsim5$ cm^2 J^{-1} and saturation of the ionization process.[36,37] This saturation ensured a uniform detection efficiency for all m states of the H atom photofragments. The use of the same laser pulse for both the state preparation and dissociation steps restricted the experimental geometry to be cylindrically symmetric with respect to the polarization direction. The polarization direction of the laser was chosen to lie in the plane of the detector; the resulting two-dimensional image was therefore a projec-

TABLE I. Comparison of experimental and theoretically modeled anisotropy parameters. The values given above have been normalized to $\beta_0 = 1$.

	β_2	β_4	β_6
	Experiment		
$HCl(E) \rightarrow H + Cl(^2P_{1/2})$	1.04(8)	−0.67(11)	0.03(13)
$HBr(H) \rightarrow H + Br(^2P_{1/2})$	1.55(4)	−0.28(9)	−0.04(7)
$HBr(H) \rightarrow H + Br(^2P_{3/2})$	1.08(6)	−0.31(9)	−0.05(11)
	Model		
A	1.299	−0.935	0.000
B	−1.303	0.303	0.000
C	2.709	0.946	0.000
D	0.055	−1.055	0.000
E	1.734	−0.355	0.000
F	0.748	−0.673	0.000
G	1.020	−0.231	0.000

FIG. 1. Calculated excited M-state population distribution for the two-photon Q branch ($\Delta J = 0$) $X\,^1\Sigma_0 \rightarrow E\,^1\Sigma_0$ transition. The M-state relative populations are shown for the experimental situation of $J = 1$ (left) as well as $J = 10$ for illustrative purposes (right). The upper plots show the distributions for $\Omega = 0$ intermediate virtual states, and the lower plots show the distributions for $\Omega = \pm 1$ intermediate states.

tion of a cylindrically symmetric three-dimensional distribution, and this experimental arrangement allowed for the use of established techniques for three dimensional image reconstruction.[38] Representative data is shown in Figs. 2–4 and summarized in Table I. Further discussion of the experimental data is given in the following sections.

B. Theoretical model

In order to understand the form of the photofragment angular distributions, we require a model that incorporates the nature of the two-photon state preparation (Section II) and also treats the single-photon photodissociation. Assuming first a Hund's case (a) or (c) description,[39] a two-photon $X\,^1\Sigma_0 \rightarrow\,^1\Sigma_0$ excitation may in principle proceed via virtual states at the one-photon level with either $\Omega = 0$ or $\Omega = \pm 1$ character, corresponding to parallel and perpendicular transitions, respectively. These pathways for Q-branch excitation of $J_0 = 1$ may be represented as

$$X\,^1\Sigma_0(J_0=1) \rightarrow \Omega_i = 0(J_i = 0,2) \rightarrow\,^1\Sigma_0(J=1),$$

$$X\,^1\Sigma_0(J_0=1) \rightarrow \Omega_i = \pm 1(J_i = 1,2) \rightarrow\,^1\Sigma_0(J=1).$$

Here, the possible values of J_i given in parenthesis are established by the 3-j symbol in Eq. (8). In what follows, we shall refer to the first pathway as the parallel pathway, and the second as the perpendicular pathway. While it is possible to determine the relative contributions of these pathways by comparing measurements made with linearly and circularly polarized light,[33] we will demonstrate below that even in a single measurement with linearly polarized light, the photodissociation of the two-photon prepared state reveals detailed information regarding the branching between the two pathways.

In Fig. 1, we plot calculated M populations for a Q branch $\Sigma_0 \rightarrow \Sigma_0$ two-photon excitation for a both a purely parallel excitation pathway and a purely perpendicular pathway. Clearly, the symmetry of the one-photon intermediate state dramatically influences the distribution. In the most general case a coherent mixture of both pathways will be active in the two-photon excitation. In principle, it is therefore necessary to know the amplitudes and phases of the radial transition dipole matrix elements for these different pathways in order to use Eq. (3) to calculate the angular
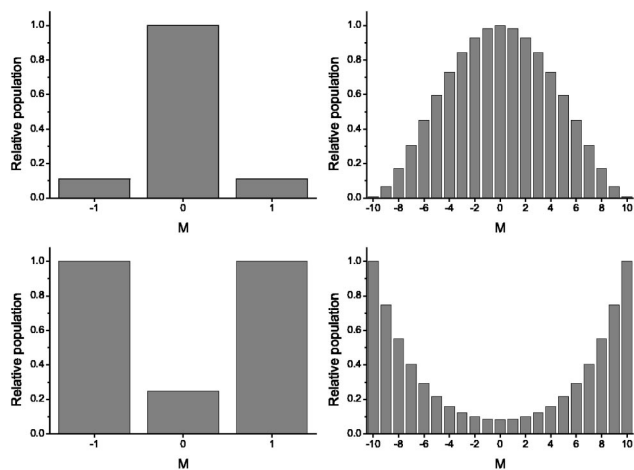
momentum polarization. Since the angular momentum polarization determines the laboratory frame distribution of molecular axes, it is anticipated that the photofragment angular distribution following axial photodissociation of the two-photon prepared state will directly reflect the nature of the two-photon excitation.

In order to interpret the H atom photofragment angular distributions resulting from single-photon dissociation of HCl and HBr prepared via two-photon excitation, we require an expression which relates the photofragment angular distribution to the angular momentum polarization in the two-photon prepared state. Rewriting Eq. (2.30) of Underwood and Powis[12] for the specific case of $J = 1$ and linearly polarized photolysis light gives

$$I(\theta) = \frac{1}{4\pi} \sum_{L=0,2,4} \beta_L P_L(\cos\theta), \tag{10}$$

where

$$
\begin{aligned}
\beta_L \propto [L] \sum_{K=0,2} [K]^{1/2} \begin{pmatrix} 1 & 1 & K \\ 0 & 0 & 0 \end{pmatrix} T_{K0} \\
\times \sum_{P=0,2} [P] \begin{pmatrix} P & K & L \\ 0 & 0 & 0 \end{pmatrix}^2 \begin{pmatrix} 1 & 1 & P \\ 0 & 0 & 0 \end{pmatrix} \\
\times \sum_q \begin{pmatrix} 1 & 1 & P \\ q & -q & 0 \end{pmatrix} |M(q)|^2.
\end{aligned}
\tag{11}
$$

We note that the sum over K in this equation is limited to $K = 0,2$, since for $J = 1$, only multipole moments of these values of K are nonzero.[34] In this equation, $M(q)$ contain the dynamical matrix elements for the photodissociation.[12] A parallel dissociation corresponds to $q = 0$, while a perpendicular dissociation corresponds to $q = \pm 1$. It follows from Eq. (11) that different possible dissociation processes contribute incoherently to the expression for the angular distribution.

TABLE II. Dynamical parameters used for the models. The second and third columns detail the radial dipole integrals for the two-photon state preparation; the superscripts (1) and (2) denote the first and second photons, respectively, and we use D_i to denote the denominator appearing in Eq. (9). The fourth and fifth columns detail the squared dissociation dynamical parameters in Eq. (11).

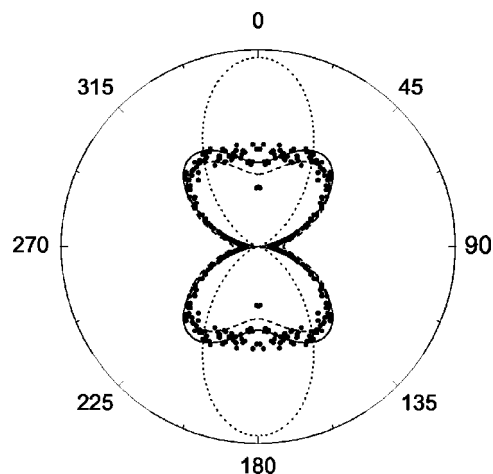| Model	$R_{0\pm1}^{(2)}R_{\pm10}^{(1)}/D_i$	$R_{00}^{(2)}R_{00}^{(1)}/D_i$	$|M(0)|^2$	$|M(\pm1)|^2$
A	1.0	0.0	1.0	0.0
B	1.0	0.0	0.0	1.0
C	0.0	1.0	1.0	0.0
D	0.0	1.0	0.0	1.0
E	$\sqrt{0.8}$	$\sqrt{0.2}$i	1.0	0.0
F	1.0	0.0	0.92	0.08
G	$\sqrt{0.8}$	$\sqrt{0.2}$i	0.88	0.12

FIG. 2. H atom photofragment angular distribution for the Cl($^2P_{1/2}$) channel from single-photon photodissociation of the two-photon state selected ($v=0, J=1$) E state of HCl. Experimental data points are shown, as well as calculated distributions for models A (solid line), C (dotted line), and F (dashed line) from Table II. The distributions shown are normalized to unit area, and the experimental data points have been symmetrized.

To interpret the experimental data requires (a) the relative values of the complex radial dipole integrals for the two-photon absorption, $R_{0\Omega_i}^{(2)}R_{\Omega_i0}^{(1)}/D_i$ [where D_i denotes the denominator appearing in Eq. (9)], and (b) the real valued squared relative dynamical parameters describing the single-photon photodissociation, $|M(q)|^2$. To proceed we therefore use a number of models for these dynamical parameters, detailed in Table II. Models A and B describe purely perpendicular two-photon excitation followed by parallel and perpendicular dissociation, respectively. Models C and D describe parallel two-photon excitation followed by parallel and perpendicular dissociation, respectively. In model E we admix 20% of a parallel two-photon step to model A with a relative phase difference of $\pi/2$. In model F 8% of perpendicular dissociation is added to model A, and in model G 12% perpendicular dissociation is added to model E. Equations (3) and (9) are used to calculate the multipole moments, T_{K0}. In Eq. (9) terms with $\Omega_i=0$ are nonzero for $J_i=0,2$, and terms with $\Omega_i=\pm1$ are nonzero for $J_i=1,2$. Eq. (11) is then used to calculate the β_L values detailed in Table I. The calculated angular distributions plotted in Figs. 2–4 are calculated using Eq. (10).

C. Photodissociation of HCl

We consider first the single-photon dissociation of HCl prepared in the $E\ '\Sigma_{0+}^+$ state via Q-branch two-photon state selection of the ($v=0, J=1$) state. For two-photon excitation of HCl to the $E\ '\Sigma_{0+}^+$ state at $2\times41\,866.0\ \text{cm}^{-1}$, the dominant intermediate virtual state is expected to be the repulsive $A\ ^1\Pi_1$ state that gives rise to the broad absorption feature centered at around 240 nm.[39,40] Absorption of a third photon at $41\,866.0\ \text{cm}^{-1}$ causes dissociation of HCl into H*($n=2$) and Cl($^2P_{1/2}$) as well as a second minor channel producing spin-orbit ground state Cl($^2P_{3/2}$). Other product channels are also observed but are not treated in this paper.[13] The dissociative state producing spin-orbit excited state Cl($^2P_{1/2}$) is a superexcited $^1\Sigma_0$ state which is a member of the Rydberg series that converges to the $A^2\Sigma$ state of the molecular ion.[13] Analysis of the dissociative $^1\Sigma_0$ potential showed that, at the photon energies considered here, dissociation is rapid and axial.[13] The channel resulting in spin-orbit ground state Cl($^2P_{3/2}$) proved too weak for quantitative analysis and was only partially resolvable from the Cl($^2P_{1/2}$)

channel.[13] In Fig. 2 we show the experimentally observed H fragment angular distribution for the Cl($^2P_{1/2}$) channel, and the β_L coefficients from a fit to Eq. (10) are detailed in Table I. In this table we also give the β_L coefficients for different combinations of the dynamical parameters for the two-photon absorption and for the photodissociation as detailed in Table II. Any effects due to hyperfine depolarization were neglected as these would be negligible under the current experimental conditions, where photodissociation of the prepared $E\ '\Sigma_{0+}^+$ state occurs on a time scale much faster than that of hyperfine depolarization.[41,42] It is found that model A, which corresponds to a purely perpendicular two-photon excitation and a parallel dissociation, provides the best fit to the experimental data. Although the experimentally observed β_L parameters are smaller in magnitude than those for model A,
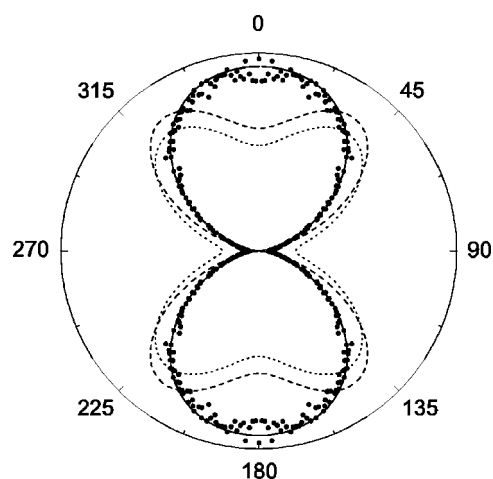

FIG. 3. H atom photofragment angular distribution from single-photon photodissociation of the two-photon state selected ($v=0, J=1$) H state of HBr, Br($^2P_{1/2}$) channel. Experimental data points are shown, as well as calculated distributions using models E (solid line), F (dotted line), and A (dashed line) from Table II. The distributions shown are normalized to unit area, and the experimental data points have been symmetrized.

J. Chem. Phys., Vol. 121, No. 23, 15 December 2004
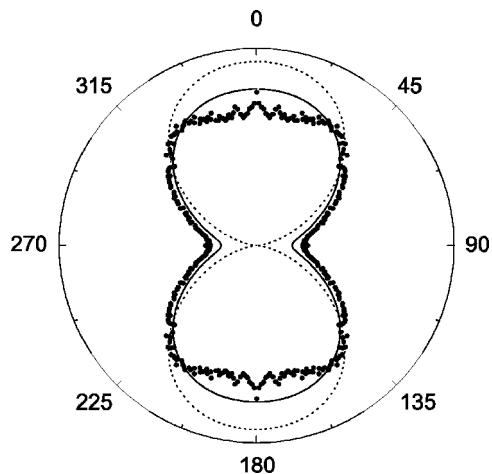
Two-photon state selection 11807

FIG. 4. H atom photofragment angular distribution from single-photon photodissociation of the two-photon state selected ($v=0,J=1$) H state of HBr, Br($^2P_{3/2}$) channel. Experimental data points are shown, as well as calculated distributions using models G (solid line) and E (dotted line) from Table II. The distributions shown are normalized to unit area, and the experimental data points have been symmetrized.

it is apparent from this table that the addition of some parallel channel character to the two-photon excitation (model E) serves only to worsen the agreement. We can also exclude the possibility that the dissociation step is saturated, since the onset of saturation would reduce the magnitude of β_4 towards zero more rapidly than β_2. It is highly likely that the reduction of the observed β_L parameters from those predicted by model A is due to an experimental artifact resulting from the difficulty of subtraction of the (isotropic) nonresonant background signal. It is informative to compare the ratio β_4/β_2 which is independent of any isotropic contributions to the signal. For model A we find $\beta_4/\beta_2=-0.720$ which is in good agreement with the data for the Cl($^2P_{1/2}$) channel for which $\beta_4/\beta_2=-0.64(15)$. Nonetheless, model F shows that there may be a minor perpendicular dissociation channel present, and this may reflect the small contribution to the signal from the partially unresolved ground state Cl($^2P_{3/2}$) channel.

D. Photodissociation of HBr

We now consider the single-photon dissociation of HBr prepared in the $H\,'\Sigma_{0+}^+$ state via Q-branch two-photon state selection of the ($v=0,J=1$) at 39 821.5 cm^{-1}.[14] The larger spin-orbit interaction in HBr compared to HCl results in a departure from a Hund's case (a) description with the result that, for the perpendicular two-photon pathway, both the $^1\Pi_1$ and $^3\Pi_1$ states are able to contribute.[43–45] More importantly, for the parallel pathway, the $^3\Pi_0$ ($\Omega=0$) intermediate state gains strength through spin-orbit mixing with the ground state. In the single-photon A-band absorption spectrum of HBr centered around 243 nm one can hence find a considerable parallel component.[46,45] This contribution was reported to be between 8% and 20% in theoretical and experimental studies.[44–46] Following the two-photon state selection, absorption of a third photon causes dissociation of HBr into H*($n=2$) and Br($^2P_{1/2}$) as well as a second weaker channel producing spin-orbit ground state Br($^2P_{3/2}$). Other channels

are also observed but are not treated in this paper.[14] The spin-orbit ground state channel was readily resolved and was significant enough to allow for quantitative analysis given below. In Figs. 3 and 4 we show H atom photofragment angular distributions for the Br($^2P_{1/2}$) and Br($^2P_{3/2}$) channels, respectively, and the results of fits to Eq. (10) are detailed in Table I.

For the Br($^2P_{1/2}$) channel, we find that the experimental data are not well represented by a perpendicular two-photon excitation and a parallel dissociation (model A), as was used for the analogous Cl($^2P_{1/2}$) data discussed above. Rather, the Br($^2P_{1/2}$) channel data are well represented by a model which allows for a 20% parallel pathway contribution to the two-photon excitation due to the $^3\Pi_0$ state,[47] followed by a parallel photodissociation via a $\Omega=0$ state (model E), as illustrated in Fig. 3 and detailed in Table I. It is found that the transition amplitude for the parallel two-photon pathway needs to be pure imaginary for good agreement with the experimental data indicating a phase difference of $\pi/2$ between the parallel and perpendicular pathways. This demonstrates the pathway-phase sensitive nature of the photodissociation process with respect to the two-photon state selection. This magnitude is in reasonable agreement with the previously reported parallel contribution to the single-photon absorption at $\sim$243 nm.[43–45] The numerical difference in the magnitude of the corresponding spatial anisotropy parameters between the experiment and model E can be partially attributed to the isotropic background and the probable contamination by a signal from $H\,'\Sigma_{0+}^+$ state $J=0$ molecules that will tend to drive the beta parameters towards 0. Nonetheless, the agreement is good, and the experimentally observed value of β_4/β_2 of $-0.18(6)$ is in good agreement with that of model E, -0.20.

Comparison of the experimentally observed H atom photofragment angular distribution for the Br($^2P_{3/2}$) channel in Fig. 4 with that for the Br($^2P_{1/2}$) channel (Fig. 3) shows a significant difference in the dissociation dynamics for the two channels. The two-photon state selection dynamics are necessarily the same for both spin-orbit channels, and it is found that adding a 12% perpendicular dissociation channel contribution to model E[48] (denoted model G) reproduces the fitted β_L values well, see Fig. 1 and Table I. The experimentally determined value of $\beta_4/\beta_2=-0.29(10)$ also agrees well with that for model G -0.23. The fact that a good fit to the Br($^2P_{3/2}$) data requires additional perpendicular dissociation character could be due to more than one active dissociative electronic state, or more complicated dissociation dynamics involving a longer lived predissociative state. This remains an open question for future study.

In summary, we have used the formalism presented in Sec. II together with knowledge of the photodissociation dynamics for the production of Cl($^2P_{1/2}$) and Br($^2P_{1/2}$) to characterize the two-photon transitions to the $E\,'\Sigma_{0+}^+$ state of HCl and the $H\,'\Sigma_{0+}^+$ state of HBr. Furthermore, we have used this knowledge of the two-photon transition to the $H\,'\Sigma_{0+}^+$ state of HBr to gain information on the weaker Br($^2P_{3/2}$) photodissociation channel.

IV. CONCLUSION

We have presented a formalism for describing the angular momentum polarization produced by two-photon absorption and applied it to a theoretical analysis of angular resolved data from the single-photon photodissociation of a two-photon aligned state in HCl and HBr. We have shown that, based only on data obtained with linear polarization, it is possible to identify the nature of the one-photon intermediate in two-photon excitation as well as that of the dissociative state. Additionally we have shown that this technique is sensitive to the phase differences between two-photon excitation pathways.

Through examination of the H atom photofragment angular distributions for the $Cl(^2P_{1/2})$ channel from photodissociation of the $(v=0, J=1)$ $E\ '\Sigma^+_{0+}$ state of HCl, we have (i) confirmed that the intermediate state in the Q-branch two-photon excitation at 83 772.0 cm^{-1} is of $^1\Pi_1$ character and (ii) confirmed that the dissociative state accessed by a third photon at 41 866.0 cm^{-1} is $\Omega=0$, and, most probably, $^1\Sigma_0$, for the $Cl(^2P_{1/2})$ channel.

Through examination of the H atom photofragment angular distributions for the $Br(^2P_{1/2})$ channel from photodissociation of the $(v=0, J=1)$ $H\ '\Sigma^+_{0+}$ state of HBr, we have found (i) that the intermediate state character in the Q-branch two-photon excitation at 79 643.0 cm^{-1} is predominantly $^1\Pi_1$ with about 20% contribution from a $^3\Pi_0$ state and (ii) confirmed that the dissociative state accessed by a third photon at 39 821.5 cm^{-1} is $\Omega=0$ for the $Br(^2P_{1/2})$ channel. Additionally, we have shown that the $Br(^2P_{3/2})$ photodissociation channel at the same energy accessed through the same two-photon transition to the $H\ '\Sigma^+_{0+}$ state shows significantly less anisotropy in the H atom photofragment angular distribution indicating either a predissociative state, or the activity of a perpendicular dissociation channel in addition to the parallel dissociation channel.

The work presented here is readily extended in a number of directions. The use of linearly polarized light and non-Q-branch transitions, or, alternatively, circularly polarized light for the two-photon state selection ensures that the angular momentum polarization in the prepared state is known analytically. By utilizing a second laser for the photolysis step, it would be possible to explore the effects of breaking the cylindrical symmetry of the experiment and also accessing different dissociation continua. Furthermore, analysis of the photoelectron angular distributions from ionization of the fragment will yield information regarding the angular momentum polarization of the photofragments in the recoil frame.

APPENDIX A: ANGULAR MOMENTUM ALGEBRA

The dot product of the electric field with the transition dipole moment in the lab frame may be decomposed into spherical vector components as[49]

$$\mathbf{d} \cdot \mathbf{e} = \sum_p (-1)^p d_p e_{-p}. \tag{A1}$$

The index p describes the polarization state of the light, where $p=0$ for linearly polarized light, and $p=\pm 1$ for circularly polarized light.

Using the Wigner-Eckart theorem[49] to separate the geometry from the dynamics for the transition dipole matrix elements in Eq. (1) gives

$$
\begin{aligned}
{}^{J'J}\rho_{M'M} = &\sum_{M_0} \sum_{n_i J_i M_i} \sum_{n'_i J'_i M'_i} \sum_{pp'} \sum_{p''p'''} (-1)^{J'-M'+J'_i-M'_i} \begin{pmatrix} J' & 1 & J'_i \\ -M' & p & M'_i \end{pmatrix} \begin{pmatrix} J'_i & 1 & J_0 \\ -M'_i & p' & M_0 \end{pmatrix} \\
&\times (-1)^{p+p'} e_{-p} e_{-p'} \frac{\langle nJ'\|\mathbf{d}\|n'_i J'_i\rangle \langle n'_i J'_i\|\mathbf{d}\|n_0 J_0\rangle}{E_{n'_i J'_i} - E_{h\nu} + i\Gamma_{n'_i J'_i}/2} (-1)^{J_0-M_0+J_i-M_i} \begin{pmatrix} J_0 & 1 & J_i \\ -M_0 & p'' & M_i \end{pmatrix} \begin{pmatrix} J_i & 1 & J \\ -M_i & p''' & M \end{pmatrix} \\
&\times (-1)^{p''+p'''} e^*_{-p''} e^*_{-p'''} \frac{\langle n_0 J_0\|\mathbf{d}\|n_i J_i\rangle \langle n_i J_i\|\mathbf{d}\|nJ\rangle}{E_{n_i J_i} - E_{h\nu} - i\Gamma_{n_i J_i}/2}.
\end{aligned} \tag{A2}
$$

Substituting this expression into Eq. (2) and using Eqs. (4.15) and (4.16) of Zare[49] to remove the summations over M_i, M'_i, M_0, M and M' gives

$$
\begin{aligned}
{}^{J'J}T_{KQ} = &(-1)^{2J+Q}[K]^{1/2} \sum_{J_i J'_i} \sum_{k_1 k_2} \begin{Bmatrix} 1 & 1 & k_1 \\ J_0 & J' & J'_i \end{Bmatrix} \begin{Bmatrix} 1 & 1 & k_2 \\ J_0 & J & J_i \end{Bmatrix} \begin{Bmatrix} k_1 & k_2 & K \\ J & J' & J_0 \end{Bmatrix} \\
&\times \sum_{pp'} \sum_{p''p'''} \sum_{n_i n'_i} (-1)^{k_1+k_2} [k_1, k_2] \begin{pmatrix} 1 & 1 & k_1 \\ p & p' & q_1 \end{pmatrix} \begin{pmatrix} 1 & 1 & k_2 \\ p'' & p''' & q_2 \end{pmatrix} \begin{pmatrix} k_1 & k_2 & K \\ q_1 & q_2 & Q \end{pmatrix} \\
&\times e_{-p} e_{-p'} e^*_{-p''} e^*_{-p'''} \frac{\langle nJ'\|\mathbf{d}\|n'_i J'_i\rangle \langle n'_i J'_i\|\mathbf{d}\|n_0 J_0\rangle}{E_{n'_i J'_i} - E_{h\nu} + i\Gamma_{n'_i J'_i}/2} \frac{\langle n_0 J_0\|\mathbf{d}\|n_i J_i\rangle \langle n_i J_i\|\mathbf{d}\|nJ\rangle}{E_{n_i J_i} - E_{h\nu} - i\Gamma_{n_i J_i}/2}.
\end{aligned} \tag{A3}
$$

APPENDIX B: THE LASER POLARIZATION FUNCTIONS $\mathcal{E}_Q^K(K_1, K_2)$

The complexity of Eq. (A3) can be reduced by recognizing the presence of spherical tensor contractions similar to those previously discussed in the context of two-photon excitation by Kummel, Sitz, and Zare.[30,31] These are purely geometrical factors containing all the information about the polarization state of the excitation light and are defined as

$$
\mathcal{E}_Q^K(k_1, k_2) = [[e \otimes e]^{k_1} \otimes [e^* \otimes e^*]^{k_2}]_Q^K
$$
$$
= (-1)^{k_1 - k_2 + Q} [K]^{1/2}
$$
$$
\times \sum_{q_1} \begin{pmatrix} k_1 & k_2 & K \\ q_1 & Q-q_1 & -Q \end{pmatrix}
$$
$$
\times [e \otimes e]_{q_1}^{k_1} [e^* \otimes e^*]_{Q-q_1}^{k_2}, \qquad (B1)
$$

where

$$
[e \otimes e]_q^k = (-1)^q [k]^{1/2} \sum_p \begin{pmatrix} 1 & 1 & k \\ p & q-p & -q \end{pmatrix} e_p e_{q-p} \qquad (B2)
$$

and

$$
[e^* \otimes e^*]_q^k = (-1)^q [k]^{1/2} \sum_p \begin{pmatrix} 1 & 1 & k \\ p & q-p & -q \end{pmatrix} e_p^* e_{q-p}^*. \qquad (B3)
$$

The tensor contraction $\mathcal{E}_Q^K(k_1, k_2)$ is related to the polarization tensor contraction $\epsilon_Q^K(k_1, k_2)$ previously discussed in the context of two-photon absorption[30,31] by the recoupling transformation

$$
\mathcal{E}_Q^K(k_1, k_2) = \sum_{k_3 k_4} \langle (11)k_3 (11)k_4 K | (11)k_1 (11)k_2 K \rangle
$$
$$
\times [[e^* \otimes e]^{k_3} \otimes [e^* \otimes e]^{k_4}]_Q^K, \qquad (B4)
$$

where $\langle (11)k_3(11)k_4 K | (11)k_1(11)k_2 K \rangle$ is readily evaluated in terms of a 9-j symbol.[49]

[1] R. N. Zare and D. R. Herschbach, Proc. IEEE **51**, 173 (1963).

[2] R. N. Zare, Mol. Photochem. **4**, 1 (1972).

[3] S. Yang and R. Bersohn, J. Chem. Phys. **61**, 4400 (1974).

[4] R. Schinke, *Photodissociation Dynamics* (Cambridge University Press, Cambridge, 1993).

[5] R. N. Dixon, J. Chem. Phys. **85**, 1866 (1986).

[6] G. E. Hall, N. Sivakumar, D. Chawla, P. L. Houston, and I. Burak, J. Chem. Phys. **88**, 3682 (1988).

[7] P. L. Houston, Acc. Chem. Res. **22**, 309 (1989).

[8] G. E. Hall and P. L. Houston, Annu. Rev. Phys. Chem. **40**, 375 (1989).

[9] A. J. R. Heck and D. W. Chandler, Annu. Rev. Phys. Chem. **46**, 335 (1995).

[10] A. T. J. B. Eppink and D. H. Parker, Rev. Sci. Instrum. **68**, 3477 (1997).

[11] L. D. A. Siebbeles and J. A. Beswick, J. Chem. Soc., Faraday Trans. **88**, 2565 (1992).

[12] J. G. Underwood and I. Powis, J. Chem. Phys. **113**, 7119 (2000).

[13] C. Romanescu, S. Manzhos, D. Boldovsky, J. Clarke, and H.-P. Loock, J. Chem. Phys. **120**, 767 (2004).

[14] C. Romanescu and H. P. Loock (unpublished).

[15] M. D. Poulsen, E. Skovsen, and H. Stapelfeldt, J. Chem. Phys. **117**, 2097 (2002).

[16] E. H. van Kleef and I. Powis, Mol. Phys. **96**, 757 (1999).

[17] M. J. Weida and C. S. Parmenter, J. Chem. Phys. **107**, 7138 (1997).

[18] R. N. Zare, Ber. Bunsenges. Phys. Chem. **86**, 422 (1982).

[19] W. Kong, Int. J. Mod. Phys. A **15**, 3471 (2001).

[20] B. Friedrich and D. R. Herschbach, Nature (London) **353**, 412 (1991).

[21] H. J. Loesch and A. Remscheid, J. Chem. Phys. **93**, 4779 (1990).

[22] H. Stapelfeldt and T. Seideman, Rev. Mod. Phys. **75**, 543 (2003).

[23] O. P. J. Vieuxmaire, M. G. D. Nix, J. A. J. Fitzpatrick, M. Beckert, R. N. Dixon, and M. N. R. Ashfold, Phys. Chem. Chem. Phys. **6**, 543 (2004).

[24] A. J. Orr-Ewing and R. N. Zare, Annu. Rev. Phys. Chem. **45**, 315 (1994).

[25] C. H. Greene and R. N. Zare, J. Chem. Phys. **78**, 6741 (1983).

[26] A. C. Kummel, G. O. Sitz, and R. N. Zare, J. Chem. Phys. **88**, 7357 (1988).

[27] A. J. Bain and A. J. McCaffery, J. Chem. Phys. **83**, 2627 (1985).

[28] A. J. Bain and A. J. McCaffery, J. Chem. Phys. **83**, 2632 (1985).

[29] A. J. Bain and A. J. McCaffery, J. Chem. Phys. **83**, 2641 (1985).

[30] A. C. Kummel, G. O. Sitz, and R. N. Zare, J. Chem. Phys. **85**, 6874 (1986).

[31] A. C. Kummel, G. O. Sitz, and R. N. Zare, J. Chem. Phys. **88**, 6707 (1988).

[32] Y. Mo and T. Suzuki, J. Chem. Phys. **109**, 4691 (1998).

[33] R. Bray and R. Hochstrasser, Mol. Phys. **31**, 1199 (1976).

[34] K. Blum, *Density Matrix Theory and Applications*, 2nd ed. (Plenum, New York, 1996).

[35] D. Mihalas, *Stellar Atmospheres* (Freeman, New York, 1971).

[36] D. C. Jacobs and R. N. Zare, J. Chem. Phys. **85**, 5457 (1986).

[37] D. C. Jacobs and R. N. Zare, J. Chem. Phys. **85**, 5469 (1986).

[38] S. Manzhos and H.-P. Loock, Comput. Phys. Commun. **154**, 76 (2003).

[39] M. H. Alexander, B. Pouilly, and T. Duhoo, J. Chem. Phys. **99**, 1752 (1993).

[40] S. C. Givertz and G. G. Balint-Kurti, J. Chem. Soc., Faraday Trans. 2 **82**, 1231 (1986).

[41] E. W. Kaiser, J. Chem. Phys. **53**, 1686 (1970).

[42] F. C. D. Lucia, P. Helminger, and W. Gordy, Phys. Rev. A **3**, 1849 (1971).

[43] Y. Matsumi, P. K. Das, and M. Kawasaki, J. Chem. Phys. **93**, 7981 (1990).

[44] T. Kinugawa and T. Arikawa, J. Chem. Phys. **96**, 4801 (1992).

[45] P. M. Regan, S. R. Langford, A. J. Orr-Ewing, and M. R. Ashfold, J. Chem. Phys. **110**, 281 (1999).

[46] G. Peoux, M. Monnerville, T. Duhoo, and B. Pouilly, J. Chem. Phys. **107**, 70 (1997).

[47] When referring to pathway contribution to the two-photon absorption, strictly we are referring to the relative magnitudes of the radial matrix element products $|R_{\Omega,\Omega_i}^2 R_{\Omega_i,\Omega_0}^1 / D_i|^2$.

[48] When referring to pathway contribution to the single-photon dissociation, strictly we are referring to the relative magnitudes of the dynamical parameters $|M(q)|^2$.

[49] R. N. Zare, *Angular Momentum* (Wiley, New York, 1988).